Journal of Materials Chemistry A

COMMUNICATION

View Article Online
View Journal | View Issue

Cite this: J. Mater. Chem. A, 2017, 5, 18448

Received 12th July 2017
Accepted 15th August 2017

DOI: 10.1039/c7ta06036j

rsc.li/materials-a

Rational design of multi-shelled CoO/Co_9S_8 hollow microspheres for high-performance hybrid supercapacitors†

Yaping Wang,[ab] Ting Zhu,*[a] Yifang Zhang,[a] Xiangzhong Kong,[a] Shuquan Liang,[a] Guozhong Cao[c] and Anqiang Pan*[a]

Hollow structures with complex interiors are promising to endow electroactive materials with fascinating physical properties, such as low mass density, large surface area and high permeability. Meanwhile, the construction of hollow structures with binary chemical compositions could further enhance the resultant electrochemical properties. Herein, we reported a designed synthesis of multi-shelled CoO/Co_9S_8 hollow microspheres by calcining a hollow microsphere precursor with S powder in argon gas (Ar). The inherent characteristic of cobalt(II) mono-oxide can benefit the electrochemical activity, while the cobalt sulfide component could improve the electrical conductivity of this cobalt-based composite material. These multi-shelled hollow structures are proved to possess a porous texture with a relatively large specific surface area (SSA = 43.1 m^2 g^{-1}), which could provide more active sites for electrochemical reactions. As a result, the as-prepared multi-shelled CoO/Co_9S_8 hollow microspheres exhibit an enhanced specific capacitance and excellent rate performance when evaluated as electrode materials for hybrid supercapacitors.

Introduction

Electrochemical capacitors (ECs)/supercapacitors have attracted great attention due to their huge advantages over conventional capacitors, such as higher specific capacitance, higher power density and much longer cycle life.[1,2] Cobalt oxides are widely reported as one of the battery-type electrode materials for hybrid supercapacitors because of their high electroactivity, high availability and low cost.[3] It has also been demonstrated that the electrochemical performances are highly dependent on the chemical compositions and microstructures of the electrode materials, and hence many previous reports have studied and developed various cobalt oxides, such as nanocones,[4] hollow boxes,[5] nanocages,[6,7] 3D-nanonet hollow structured Co_3O_4,[8] hollow octahedral,[9] and cobalt hydroxideoxide hexagonal ring-graphene hybrids.[10] We previously reported a template approach to prepare multi-shelled hollow Co_3O_4 microspheres, which exhibit good supercapacitive performance.[11] Despite the advantages of Co_3O_4, the reported electrochemical performances are still far from satisfactory. The modulation of chemical compositions could be one of the effective approaches to improve the electrochemical properties of hybrid supercapacitors. Cobalt monoxide (CoO) has a higher cobalt content than Co_3O_4, making it a better choice than pure Co_3O_4 for redox reactions.[12,13] Therefore, the reduction of Co_3O_4 to CoO may be an effective way to enhance the pristine specific capacitance of a cobalt based composite material. However, the poor electrical/ionic conductivity of cobalt oxides has resulted in practical capacitances much lower than the theoretical ones, which restricts their rate performances.[14,15] Many previous reports have used an ion-exchange method to introduce beneficial ions into the host material to improve the electrical conductivity.[16–19] For example, the substitution of O ions with S ions can be employed to improve the conductivity because cobalt sulfides usually exhibit smaller band-gap energy and hence higher electrical conductivity owing to the more covalent metal–sulfur bond.[20,21] Zeng *et al.* reported a lower charge-transfer resistance and better capacitive characteristic of CoS nanowire@$NiCo_2S_4$ sheet arrays than CoO@$NiCo_2O_4$.[22] Tang *et al.* also reported a higher electrical conductivity and faster charge transfer of $Co_{1.5}Ni_{1.5}S_4$ than cobalt–nickel hydroxides and oxides.[23] Although the sulfurization could improve the conductivity of oxide materials, the introduction of S to replace O may blemish the specific capacitance. Therefore, a partial substitution of O ions to produce cobalt oxides/sulfide composites may be a better alternative. The proportion of cobalt sulfide in the composites may be essential to optimize the electrochemical properties of cobalt oxides/sulfide composites.

[a]School of Materials Science and Engineering, Central South University, Changsha 410083, Hunan, China. E-mail: pananqiang@csu.edu.cn; Zhut0002@csu.edu.cn; Fax: +86-0731-88876692

[b]Light Alloy Research Institute, Central South University, Changsha 410083, Hunan, China

[c]Department of Materials Science and Engineering, University of Washington, Seattle, WA, 98195, USA

† Electronic supplementary information (ESI) available. See DOI: 10.1039/c7ta06036j

Many studies have reported the construction of hierarchical structures with the integration of different chemical compositions to achieve unique physical and chemical properties.[24–27] Dong *et al.* fabricated ZnO nanoparticle-loaded CuO dandelion hierarchical structures to facilitate charge transfer within the composite.[28] Chang *et al.* reported an ultrafast charge transfer in $Co_3O_4/BiVO_4$ heterostructures owing to the synergetic enhancement of surface reaction kinetics by introducing discrete nanoisland p-type Co_3O_4 onto n-type $BiVO_4$.[29] As 3D architectures, hollow micro-/nanostructures with complex interiors such as multi-shelled structures are receiving increasing research attention for application in supercapacitors because the combined hollow void spaces could provide more electroactive sites for electrochemical reactions. In addition, the space between neighboring shells of these structures can hold electrolyte ions and thus facilitate charge transport.[30–32]

Therefore, the design and fabrication of a complex architecture by employing a cobalt oxides/sulfide hybrid might be a feasible strategy to obtain unique electrochemical properties. Herein, we fabricated a series of cobalt based composites with different compositions as electrode materials for supercapacitors. $Co_2CO_3(OH)_2$ nanorods were first grown on carbon microspheres by a facile low-temperature solution route. Then Co_3O_4 multi-shelled hollow microspheres were obtained by annealing the $Co_2CO_3(OH)_2$ precursor in air and later used as the template to fabricate CoO/Co_9S_8 multi-shelled hollow microspheres by annealing with S powder in Ar gas. The compositions of the products can be controlled by calcining Co_3O_4 and S at different ratios. Owing to the unique morphology and synergistic effect of CoO and Co_9S_8, the obtained CoO/Co_9S_8 exhibited the highest capacitance and remarkable high-rate capability among all the samples.

Experimental

Material synthesis

All the solvents and chemicals were of reagent grade and used without further purification. The carbon spheres (CSs) were synthesized according to a method in a previous report.[33] To prepare the $CS@Co_2CO_3(OH)_2$ core-shelled composite, 50 mg of carbon spheres were dispersed into 100 ml of a mixed solvent of water and alcohol (1 : 1, v/v) by ultrasonication for 0.5 h. Next, 1 g urea and 0.2 g $Co(NO_3)_2 \cdot 6H_2O$ were added to the solution. After stirring for 12 h at 80 °C in an oil bath, the obtained products were collected by centrifugation and washed with water and alcohol, followed by drying at 60 °C for 12 h. The precursor can be completely converted into multi-shelled Co_3O_4 hollow microspheres by a heat treatment at 450 °C in air for 2 h with a heating ramp rate of 3 °C min^{-1}. The Co_3O_4 hollow microspheres were mixed with S powder with different molar ratios (Co : S with ratios of 1 : 1, 1 : 4 or 1 : 8) and annealed at 400 °C for 4 h under Ar gas flow in a furnace to prepare multi-shelled cobalt monoxide/sulfide hollow microspheres. Multi-shelled CoO microspheres were prepared by annealing Co_3O_4 without adding S powder in a H_2/Ar (5 : 95, v/v) atmosphere. Core-shelled CoO was also prepared for comparison by directly annealing the $CS@Co_2CO_3(OH)_2$ precursor in an Ar atmosphere.

Characterization

The main text of the article should appear here with headings as appropriate. The crystalline structures of the as-prepared samples were characterized by X-ray diffraction (XRD, Rigaku D/max 2500, Cu Kα radiation, $\lambda = 0.1518$ nm). The morphologies were detected using a scanning electron microscope (SEM, Quanta FEG 250) and transmission electron microscope (TEM, Nova NanoSEM230). Thermogravimetric analysis (TGA) was conducted on a NETZSCH STA 449C. X-ray photoelectron spectroscopy (XPS) was performed on an ESCALAB 250Xi (ThermoFisher-VG Scientific, Britain). Nitrogen adsorption–desorption measurements were conducted at 77 K (NOVA 4200e, Quantachrome Instruments).

Electrochemical measurements

The main text of the article should appear here with headings as appropriate. The working electrodes were prepared by mixing 80 wt% of active material, 10 wt% of carbon black, and 10 wt% of polyvinylidene fluoride (PVDF) in an *N*-methyl-2-pyrrolidone (NMP) solution to make a slurry. Then, it was coated onto the Ni foam substrate of 1×2 cm^2 in size and dried in a vacuum oven at 60 °C for 12 h. The mass loading was about 1 mg cm^{-2}. Electrochemical measurements were conducted in a three-electrode system in 2 M KOH electrolyte with a Pt foil as the counter electrode and Hg/HgCl as the reference electrode. Cyclic voltammetry (CV) was conducted with a CHI660C electrochemical workstation with different voltage scan rates. Electrochemical impedance spectroscopy (EIS) was performed using an Autolab electrochemical station (Metrohm) in the frequency range from 100 kHz to 10 MHz. The specific capacitances were calculated according to a charge/discharge test and the following equation:

$$C = I\Delta t / M\Delta V \quad (1)$$

where C (F g^{-1}) is the specific capacitance, I (A) represents the discharge current, Δt (s) is the discharging time, ΔV (V) is the voltage window, and M (g) is the mass of active materials.

For the fabrication of asymmetric supercapacitor (ASC) devices, the as-prepared CoO/Co_9S_8 and activated carbon were used to assemble the ASC devices in an aqueous 2 M KOH electrolyte. For good performance, the mass loading of the two electrodes was optimized by charge balance ($q^+ = q^-$). The CV curves and charge/discharge profiles were measured in a potential range of 0–1.5 V using a CHI660C workstation.

Results and discussion

Fig. 1 is a scheme showing the synthetic route for all the cobalt based composite materials. The CS templates are first prepared by a hydrothermal method using glucose as the carbon source. The subsequent core-shelled $CS@Co_2CO_3(OH)_2$ microspheres are synthesized through a low-temperature hydrothermal process, in which the precipitation of Co^{2+} takes place in the presence of urea (step I). After annealing in air, the $CS@Co_2CO_3(OH)_2$ microspheres are transformed into multi-shelled

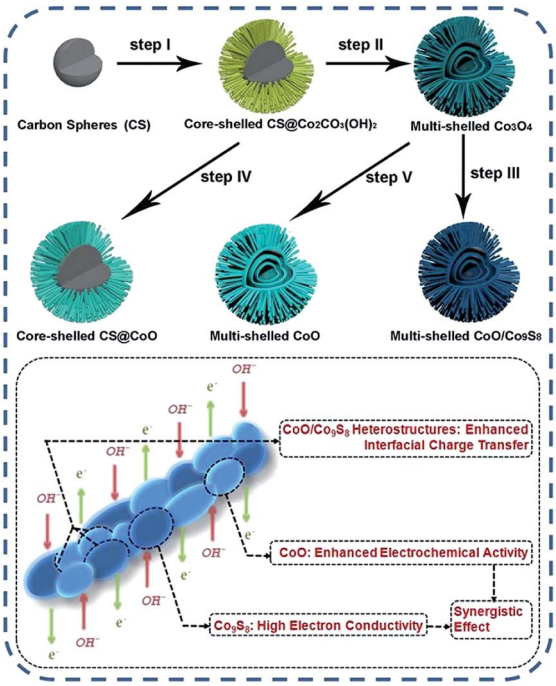

Fig. 1 Schematic illustration of the preparation of multi-shelled cobalt oxides/sulfide composite hollow structures.

Co_3O_4 hollow microspheres completely (step II). The formation of the multi-shelled structure can be ascribed to the diffusion of cobalt species into the interior of CSs. During the calcination process, the cobalt species within the carbon microspheres can shrink into multi-shells during the gradual removal of CSs. Finally, the Co_3O_4 hollow microspheres are sulfurized to CoO/Co_9S_8 hollow microspheres by annealing Co_3O_4 with S powder in an Ar atmosphere (step III). To further explore the effects of the composition and structure on electrochemical properties, core-shelled CS@CoO (by step IV) and multi-shelled CoO microspheres (by step V) are also obtained for comparison.

The morphologies of the CSs prepared by the hydrothermal method are shown in Fig. S1a and b.† The as-synthesized templates are uniform solid spheres with an average size of 1 μm. After a facile solution reaction, cobalt based precursors in nanorods have been grown against the CSs (Fig. S1c and d†). According to the XRD results shown in Fig. S2,† the patterns of precursors can be indexed to $Co_2CO_3(OH)_2$ (JCPDS card no. 48-0048). After a calcination in air, the CS@$Co_2CO_3(OH)_2$ precursors were converted to multi-shelled Co_3O_4, whose structural features can be seen clearly in Fig. S1e and f.† By heating the as-prepared multi-shelled Co_3O_4 and S powder in different molar ratios under Ar gas, cobalt based oxide/sulfide composite materials with multi-shelled hollow structures can be obtained. The TG/DSC results of the mixture of Co_3O_4 and S powder in an Ar atmosphere are shown in Fig. S3.† The endothermic peak at 114.2 °C can be attributed to sulfur melting.[34] An exothermal peak at 273.9 °C and the corresponding fast weight drop between 200 °C and 300 °C can be detected, which may be related to the reduction of Co_3O_4 by S, along with the production of sulfur oxide. The weight loss between 350 °C and 450 °C can be attributed to the evaporation of extra S. To exert the reducibility of sulfur and remove the extra S, the temperature of 400 °C was chosen for sample calcination. The XRD phases of the reduced or sulfurized Co_3O_4 are shown in Fig. S4.† The crystal phase of the reduced product obtained by annealing Co_3O_4 in a H_2/Ar atmosphere is CoO (JCPDS card no. 75-0393, $Fm\bar{3}m$ (225), $a = 0.4258$ nm) with a trace amount of Co present. When reacting Co_3O_4 with S in a molar ratio of 1 : 1 (Co : S), the main phase of CoO is remained retained except that weak diffraction peaks of CoS (JCPDS card no. 75-0605) can be detected. When the ratio is changed to 1 : 4, the products are composed of Co_9S_8 (JCPDS card no. 75-2023, $Fm\bar{3}m$ (225), $a = 9.923$) and CoO with well detected XRD peaks. By further increasing the S amount and changing the ratio to 1 : 8, the pristine cobalt oxides can be sulfurized to CoS/Co_9S_8, in which all the strong XRD peaks are mainly attributed to CoS. The products are thus named CoO, CoO/CoS, CoO/Co_9S_8 and CoS/Co_9S_8 corresponding to the molar ratios of Co : S of 1 : 0, 1 : 1, 1 : 4 or 1 : 8, respectively.

Fig. 2 displays the morphologies and structures of CoO/Co_9S_8 microspheres. From the SEM images (Fig. 2a and b), it can be seen that the nanorod-assembled exterior shell can be well preserved after sulfurization. The CoO/Co_9S_8 microspheres are uniform in size with an average diameter of 1.5 μm. The SEM results of CoO/CoS and CoS/Co_9S_8 are also displayed in Fig. S5,† which further confirm that the nanorod-assembled structure can be retained in the sulfurization process. The TEM images (Fig. 2c) of CoO/Co_9S_8 have confirmed the unique multi-shelled structures, which are well inherited from the Co_3O_4 hollow microspheres (recall Fig. S1e and f†). Triple shells can be observed in Fig. 2d, even though the boundaries of the shells are not so distinct. The unique multi-shelled structure can effectively increase the surface area of the particles and could provide more contact areas between electrode materials and electrolyte.[30,31] A Brunauer–Emmett–Teller (BET) surface area of 43.1 $m^2\ g^{-1}$ and a high pore volume of 0.29 $cm^3\ g^{-1}$ with pore sizes below 10 nm are obtained for the multi-shelled CoO/Co_9S_8 hollow spheres (Fig. S6†). In the detailed TEM image in Fig. 2e, the nanorods are found to be composed of nanoparticles with particle sizes of 20–30 nm. The further HRTEM characterization (Fig. 2f) of the nanoparticles reveals the lattice fringes with *d*-spacings of 0.5719, 0.2987, 0.2450 and 0.2122 nm, corresponding to Co_9S_8 (111) (311) and CoO (111) (200), respectively. Selected-area electron diffraction (SAED) analysis gives a pattern of several integrated circles, which can be assigned to Co_9S_8 (311) (422) (711) and CoO (111) (200), indicating the formation of polycrystalline Co_9S_8 and CoO (Fig. 2g). The elemental mapping results obtained from SEM (Fig. S7†) demonstrate that all the microspheres are partially sulfurized and the distributions of Co, S, and O elements are homogeneous within the spheres. However, the elemental mapping results obtained using the high angle annual dark-field (HAADF) technique (Fig. 2h–l) show that the surface of the pristine cobalt oxide is sulfurized more heavily because sulfur species need to travel through the shells to react with the interior species. Although the interior is less sulfurized, the elemental mapping results have demonstrated a homogeneous

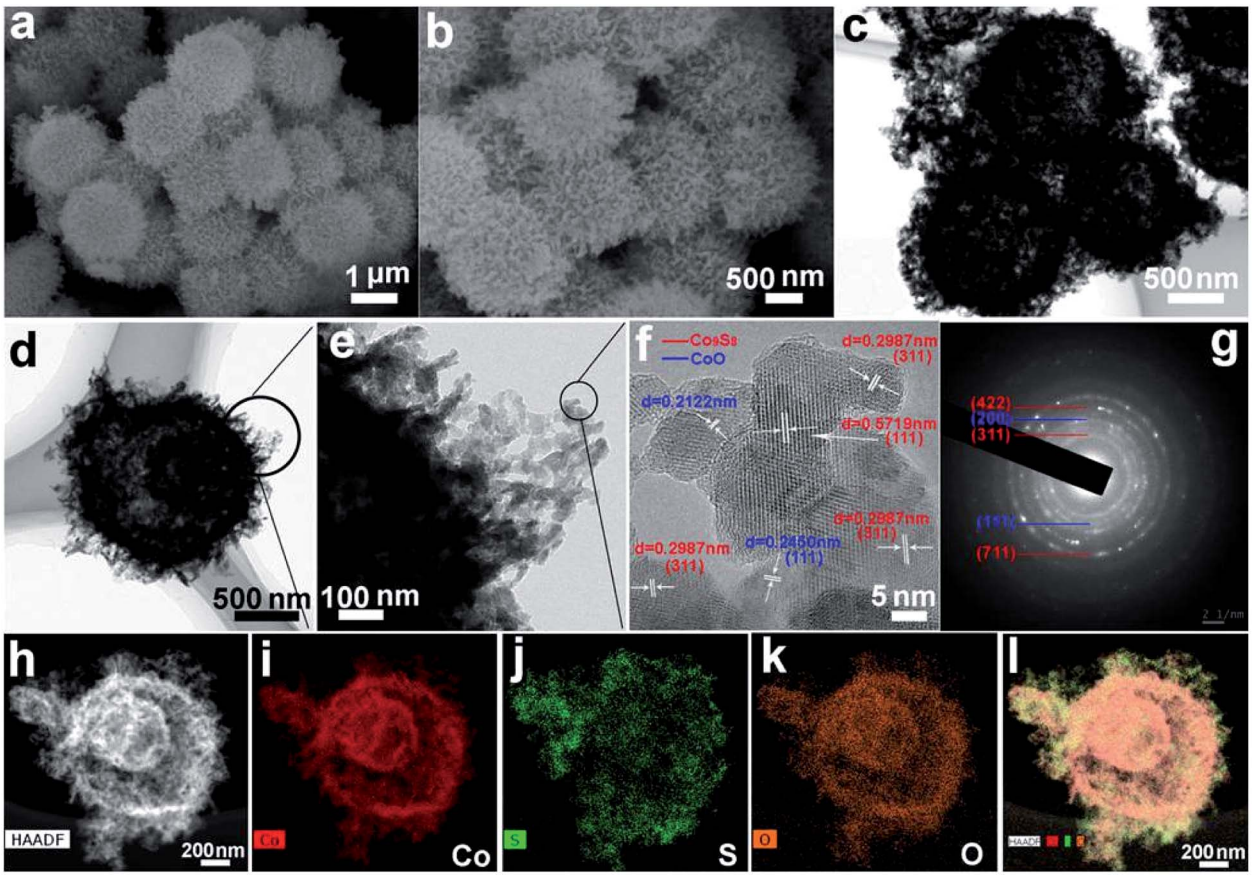

Fig. 2 SEM images (a) and (b), TEM images (c)–(e), HRTEM image (f), SAED pattern (g) and elemental mapping images (h)–(l) of the multi-shelled CoO/Co_9S_8 hollow microspheres.

distribution of Co_9S_8 in the composite. The weight percentage of Co_9S_8 in the composite was further determined from the TG curve (Fig. S8†). The weight loss below 250 °C can be ascribed to the evaporation of adsorbed water molecules. As the temperature increases to around 500 °C, the weight increase can be attributed to the gradual oxidation of cobalt sulfide to cobalt sulfate.[35] The weight decrease above 700 °C may be related to the decomposition of cobalt sulfate and the remaining cobalt sulfide into cobalt oxide. Based on the weight changes from CoO/Co_9S_8 to Co_3O_4, the weight percentage of Co_9S_8 is 22.6%. For comparison, the morphologies and structures of the core-shelled CS@CoO microspheres and the multi-shelled CoO microspheres are shown in Fig. S9 and S10,† respectively. Further XRD analysis of the products (Fig. S9a†) shows that the XRD peaks can be indexed to CoO (JCPDS card no. 75-0393, $Fm\bar{3}m$ (225), $a = 0.4258$ nm) and Co (JCPDS card no. 15-0806). The SEM images (Fig. S9b†) show that the surface of the carbon microspheres is homogeneously covered by CoO nanorods with a rough size of 1.5 μm. The enlarged SEM image (Fig. S9c†) and the TEM image (Fig. S9d†) indicate a solid sphere of the core-shelled CS@CoO. More SEM and TEM images in Fig. S10† show that the CoO microspheres have similar external and interior structures to multi-shelled CoO/Co_9S_8 microspheres.

XPS was conducted to investigate the surface chemical compositions of the CoO/Co_9S_8 sample. Fig. 3a indicates the presence of Co, S and O elements in the composite. In the XPS spectra (Fig. 3b), the binding energies at 778.5 and 793.7 eV are attributed to Co $2p_{3/2}$ and Co $2p_{1/2}$ from cobalt sulfides.[36,37] The peaks at 781.1 and 797.3 eV are related to Co $2p_{3/2}$ and Co $2p_{1/2}$

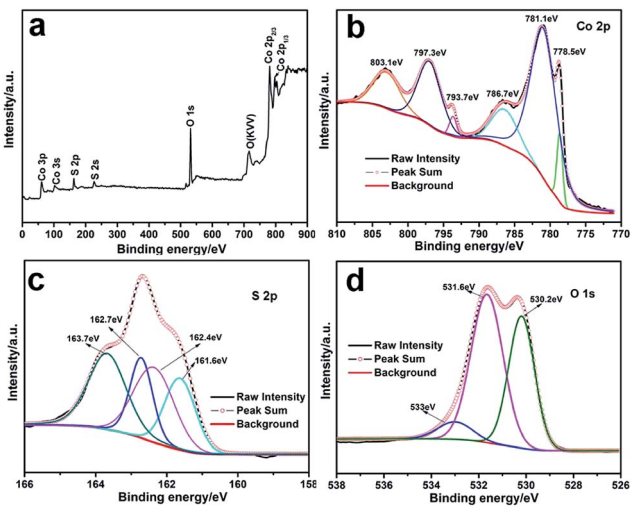

Fig. 3 Typical XPS survey spectra (a) and the corresponding Co 2p (b), S 2p (c) and O 1s (d) XPS spectra of the CoO/Co_9S_8 multi-shelled hollow microspheres.

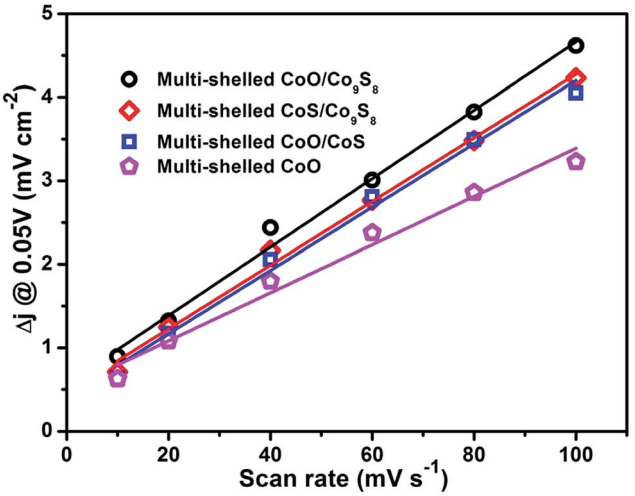

Fig. 4 Estimated ECSAs of multi-shelled cobalt oxides/sulfides composite hollow microspheres.

from Co–O. The binding energies centered at around 786.7 and 803.1 eV could be identified as the shake-up peaks of Co^{2+}. In the case of S (Fig. 3c), the peaks at 161.6 and 162.7 eV are assigned to S $2p_{3/2}$ and S $2p_{1/2}$, while the peaks at 162.4 and 163.7 eV agree with the positions of the disulfide species (S_2^{2-}), indicating that sulfur possesses multiple valences.[38] In Fig. 3d, the peaks at 530.2 and 531.6 eV can be attributed to the O 1s from the CoO and the hydroxide ions. The other peak observed at 533 eV can be assigned to a small amount of physically adsorbed water molecules.[39] The results indicate the successful formation of a cobalt oxide/sulfide composite with multiple valences, leading to complex band gaps, which is beneficial for obtaining high electrochemical activity.

To explore the electrochemical performances of the composite materials, the core-shelled CS@CoO and multi-shelled cobalt mono-oxide/sulfide hollow microspheres were assembled into a three-electrode system for measurements. First, electrochemical double-layer capacitances (C_{dl}) were measured within non-faradaic regions to evaluate the effective surface area of all the samples. Fig. 4 shows that the C_{dl} values of CoO/Co_9S_8, CoS/Co_9S_8, CoO/CoS and CoO multi-shelled microspheres calculated from the CV curves (Fig. S11†) are 40, 38, 37 and 28.8 μF cm^{-2}, respectively, indicating the increase of electrochemically active sites obtained from partial sulfurization. Fig. 5a shows CV curves of all the samples at a scan rate of 5 mV s^{-1} in the same potential window of 0–0.55 V (*vs.* the SCE). The CV curves exhibit redox peaks during the anodic and cathodic sweeps, which can be attributed to the faradaic redox reactions in the alkaline electrolyte. The possible reversible redox reactions of cobalt oxide/sulfide may be indicated by eqn (2)–(7) that are mediated by OH^- ions in the alkaline electrolyte.[15,19,36,40–43]

$$CoO + OH^- \leftrightarrow CoOOH + e^- \quad (2)$$

$$CoOOH + OH^- \leftrightarrow CoO_2 + H_2O + e^- \quad (3)$$

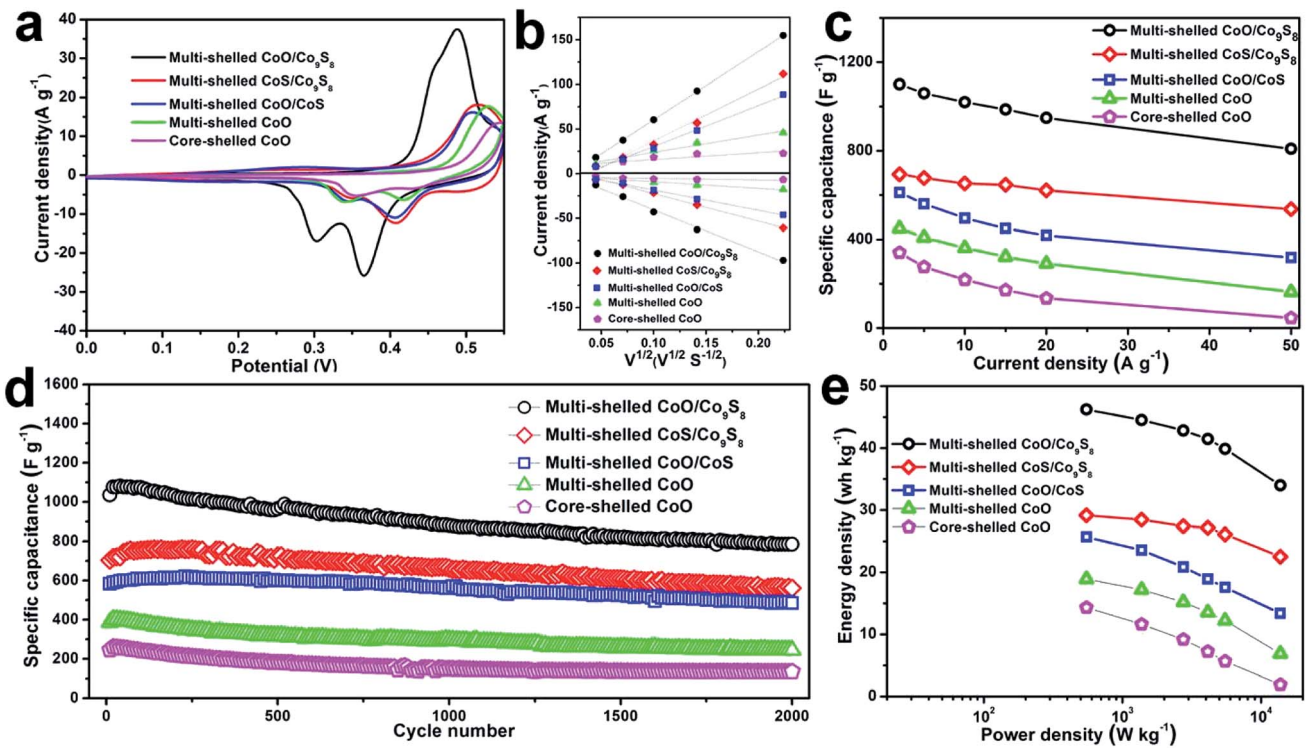

Fig. 5 CV curves obtained at 5 mV s^{-1} (a), the linear fitting of I_p *vs.* $v^{1/2}$ curves for the redox peaks (b), specific capacitances at different current densities (c), cycling performance at 5 A g^{-1} (d) and the energy densities at different power densities (e) of four multi-shelled cobalt oxides/sulfides composite hollow microspheres and CS@CoO microspheres.

$$Co_9S_8 + OH^- \leftrightarrow Co_9S_8OH + e^- \quad (4)$$

$$Co_9S_8OH + OH^- \leftrightarrow Co_9S_8O + H_2O + e^- \quad (5)$$

$$CoS + OH^- \leftrightarrow CoSOH + e^- \quad (6)$$

$$CoSOH + OH^- \leftrightarrow CoSO + H_2O + e^- \quad (7)$$

The current densities of the core-shelled CS@CoO are lowest among all the samples, indicating its poor electrochemical activity. This may be caused by its solid interior which delivers a much less surface area than those of the other samples, while the residual carbon contributed very limitedly to the over-all capacitance. All the other samples with multi-shelled structures have exhibited higher capacitance, implying the advantages of the constructed hierarchical structures. Compared to multi-shelled CoO, the areas of the CV curves are larger when introducing S ions into the composite. However, the CoS/Co_9S_8 sample delivers less capacitance than the CoO/Co_9S_8 one, which can be ascribed to the larger molecular weight of CoS than CoO. The CV curves at different scan rates of the samples are shown in Fig. S12a and S13,† respectively. It can be seen from Fig. S12a† that the CV loop at 50 mV s^{-1} is almost overlapped with the one at 20 mV s^{-1} for the core-shelled CS@CoO. At high scan rates, the electrolyte ions cannot fully access the interiors of the electrodes owing to the reduced diffusion time. However, by constructing multi-shelled hierarchical structures or introducing S ions, the redox peaks during the anodic and cathodic sweeps at high scan rates can maintain their shapes, illustrating the fast charge/discharge response (Fig. S13†). The relationship between the square root of scan rates and the corresponding peak current densities is shown in Fig. 5b. Their linear relationship indicates the good reversibility of diffusion-controlled reactions. The fitting line of CoO/Co_9S_8 microspheres has the biggest slope, which suggests their fastest reaction at high rates. The better electrical conductivity of cobalt sulfide and higher electroactivity of CoO may have led to the best performance of the CoO/Co_9S_8 composite. Fig. S12b and S14† show the charge and discharge curves of all samples at different current densities ranging from 2 to 50 A g^{-1}. The relevant capacitances of the electrodes are shown in Fig. 5c. The core-shelled CS@CoO delivers the lowest capacitance, which is consistent with the above CV analysis. The multi-shelled CoO shows a specific capacitance of 449 F g^{-1} at 2 A g^{-1}, which is higher than that of the pristine Co_3O_4 (394 F g^{-1}),[11] indicating the merits of reduction of Co_3O_4 to increase the active cobalt content. However, the capacitance of CoO is far from the theoretical value due to the poor conductivity. This can be improved by introducing S ions into the composite. Better capacitance retentions at high current densities can be delivered with higher ratios of cobalt sulfides in the composites, which can be concluded from Fig. S15†. The Nyquist plots of the five electrodes are shown in Fig. S16.† The straight lines appearing in the low frequency range represent the Warburg impedance, corresponding to the electrolyte diffusion in the porous electrode. The equivalent ohmic resistance (*e.g.*, the resistance of the electrode, electrolyte and the contact resistance between the electrode and electrolyte) of the supercapacitors can be estimated according to the *X*-intercept of the Nyquist plots in the high frequency region. The ohmic values of multi-shelled CoO/Co_9S_8, CoS/Co_9S_8, CoO/CoS, and CoO, and core-shelled CoO electrodes are 0.34, 0.41, 0.45, 0.46 and 0.45 Ω (inset of Fig. S16†), respectively, which shows the best electrical conductivity of the CoO/Co_9S_8 electrode. However, an appropriate content of cobalt sulfides is desirable to enhance the conductivity, but not deteriorate the specific capacitance too much. For multi-shelled CoO/Co_9S_8 hollow microspheres, high specific capacitances of 1100, 1060, 1020, 987 and 949 F g^{-1} can be obtained at the current densities of 2, 5, 10, 15 and 20 A g^{-1}, respectively. Even when the current density is as high as 50 A g^{-1}, a high specific capacitance of 809 F g^{-1} can still be achieved. Compared with CoS/Co_9S_8, the higher capacitance of CoO/Co_9S_8 can be attributed to the higher electroactivity of CoO than CoS, implying the construction of cobalt oxide/sulfide with adjusted components can boost the electrochemical properties by utilizing the synergistic effect of both components. Fig. 5d displays the long-term cycling stability of the electrodes at a current density of 5 A g^{-1}. After 2000 cycles, the capacitance of CoO/Co_9S_8 decreases from 1035 F g^{-1} to 785 F g^{-1}, demonstrating a good cycling stability. All the other samples also deliver good cycling stability but a lower capacitance than CoO/Co_9S_8, and their performances are consistent with the CV results and charge/discharge curves. The long-term cycling performance of CoO/Co_9S_8 at a high current density of 50 A g^{-1} is also tested and shown in Fig. S17.† The capacitance decreases in the initial stage, but it remains very stable after 500 cycles. A good capacitance retention of 83.7% can be maintained after 15 000 cycles, demonstrating the good cycling stability of the

Table 1 Electrochemical performance of the reported cobalt-based electrode materials

Materials	Capacitance (F g^{-1})	Current density (A g^{-1})	Electrolyte	Voltage window (V)
3D CoS nanoflake/Ni(OH)$_2$ nanosheet[27]	900	5	3 M KOH	0–0.5
CoS hollow structures[42]	865	5	2 M KOH	0–0.55
Co_9S_8 nanorods[44]	450	5	2 M KOH	−0.1–0.4
C@Co_9S_8 hollow sphere[45]	617	3	2 M KOH	−0.15–0.55
3D flower-like Co_9S_8 (ref. 46)	397	2	6 M KOH	0–0.55
Co_3O_4/CoO nanoparticles[47]	240	1	6 M KOH	0–0.35
Co_9S_8 nanotube[48]	285	0.5	6 M KOH	−0.1–0.5
This work:	1100	2	2 M KOH	0–0.55
CoO/Co_9S_8 heterostructure-assembled multi-shelled hollow sphere	1060	5		

electrode. Fig. 5e compares the energy density of all the samples. The CoO/Co_9S_8 sample delivers a high energy density of 46.2 W h kg^{-1} at a power density of 550 W kg^{-1} and 34 W h kg^{-1} at a high power density of 13.7 kW kg^{-1} can be maintained. While the energy densities of CoS/Co_9S_8, CoO/CoS, multi-shelled CoO and CS@CoO electrodes can be calculated to be 29.2, 25.7, 18.9 and 14.3 W h kg^{-1} at the same power density of 550 W kg^{-1}, respectively, showing the superiority of the multi-shelled CoO/Co_9S_8 over all the other samples. Table 1 lists the electrochemical performances of previously reported cobalt-based oxides and sulfides electrodes, which indicates the good properties of our heterostructured CoO/Co_9S_8 among the cobalt-based supercapacitor electrodes.

To further investigate the potential application of the CoO/Co_9S_8 electrode, ASC devices composed of a CoO/Co_9S_8 electrode and an active carbon (AC) electrode were evaluated in a 2 M KOH aqueous electrolyte. As shown in Fig. S18,† the CV curve of AC exhibits a typical capacitive behavior with a nearly rectangular shape. According to the electrochemical test results of CoO/Co_9S_8 (Fig. 5) and AC (Fig. S18†), the mass loading ratio of CoO/Co_9S_8 and AC is around 0.2. Fig. 6a shows the CV curves of the ASC device at different scan rates. Obvious redox peaks can be observed from the CV curves, showing the faradaic characteristics of all the electrode materials. The charge–discharge curves and corresponding specific capacitances of the ASC device are shown in Fig. 6b and c. The ASC device can deliver 73, 72, 69, 66, 65, 54 and 37 F g^{-1} at the current densities of 1, 2, 3, 5, 10, 20 and 50 A g^{-1}, respectively, indicating the good rate performances. Fig. 6d shows the cycling stability of the CoO/Co_9S_8||AC device at a current density of 10 A g^{-1}. After 5000 cycles, the asymmetric cell shows a high capacitance retention of 95.27%. The good supercapacitive performance of the multi-shelled CoO/Co_9S_8 hollow spheres can be attributed to the following reasons, as shown in bottom part of Fig. 1: (1) the reduction of Co_3O_4 to increase the content of active cobalt species can enhance the specific capacitance. (2) The introduction of sulfur species can improve the electrical conductivity, thus facilitating charge transport. (3) The construction of CoO/Co_9S_8 heterostructures by combining different compositions can possess different band gaps to enhance the interfacial charge transfer and surface reaction kinetics. (4) The unique multi-shelled hollow structure provides extra space between neighboring shells which can serve as a reservoir for electrolyte and increase the contact area between the electrode and electrolyte.

Conclusions

In summary, CoO/Co_9S_8 hollow microspheres with complex multi-shelled structures were synthesized using carbon spheres

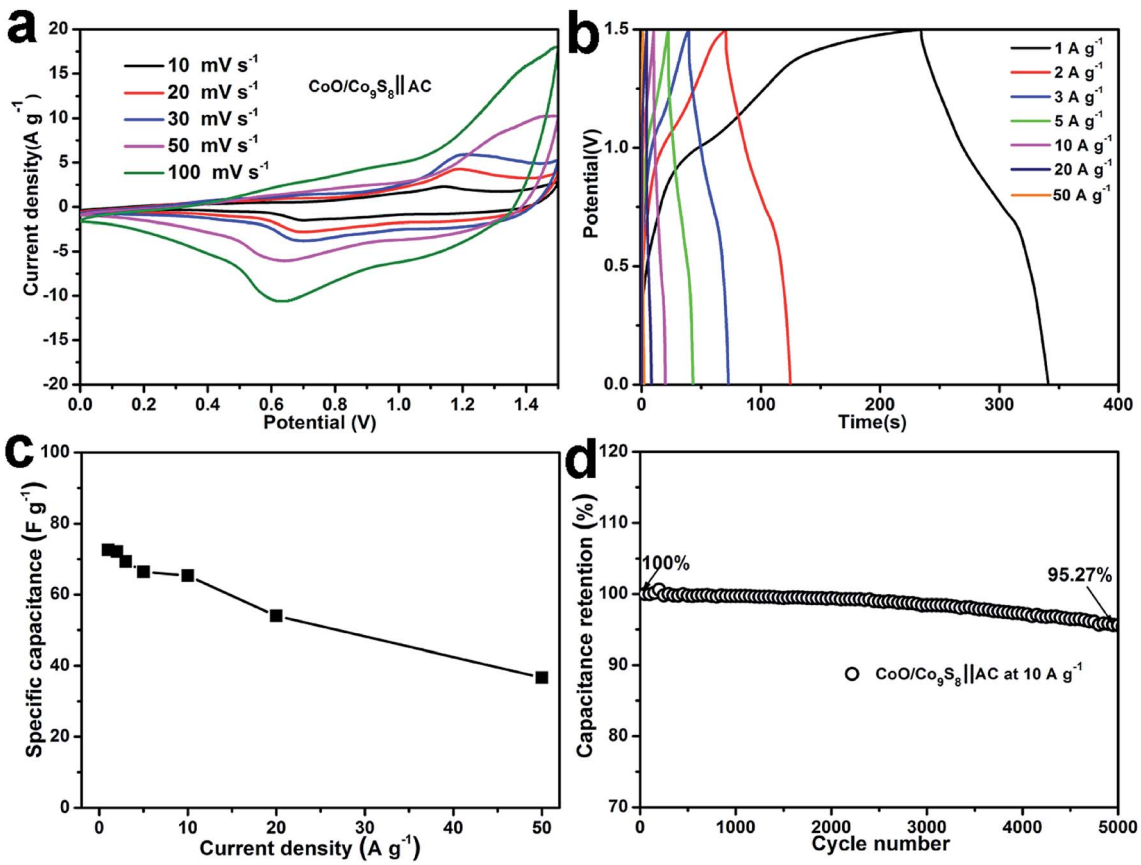

Fig. 6 CV curves at different scan rates (a), the charge–discharge profiles at different current densities (b), specific capacitances at different current densities (c), and the cycling performance at 10 A g^{-1} (d) of the CoO/Co_9S_8||AC ASC devices in a voltage window of 0–1.5 V.

as templates. $Co_2CO_3(OH)_2$ precursors were first grown on carbon microspheres by a facile low-temperature solution route. Cobalt oxide (Co_3O_4) with multi-shelled hollow microspheres was then obtained by annealing the $Co_2CO_3(OH)_2$ precursor in air. The as-synthesized Co_3O_4 was used as a template to synthesize a series of cobalt mono-oxide/sulfide complex multi-shelled hollow microspheres by reduction and S ion-exchange. The as-formed samples were tested as electrode materials for hybrid supercapacitors and the results demonstrated the best electrochemical performance of the CoO/Co_9S_8 sample.

Conflicts of interest

There are no conflicts to declare.

Acknowledgements

This work was supported by the National Natural Science Foundation of China (No. 51374255, 51302323), the Program for New Century Excellent Talents in University (NCET-13-0594), and the Innovation-driven Program of Central South University (No. 2017CX001).

References

1 G. Wang, L. Zhang and J. Zhang, *Chem. Soc. Rev.*, 2012, **41**, 797–828.
2 L. L. Zhang and X. S. Zhao, *Chem. Soc. Rev.*, 2009, **38**, 2520–2531.
3 K. K. Lee, W. S. Chin and C. H. Sow, *J. Mater. Chem. A*, 2014, **2**, 17212–17248.
4 X. Liu, R. Ma, Y. Bando and T. Sasaki, *Adv. Funct. Mater.*, 2014, **24**, 4292–4302.
5 W. Duan, Z. Hu, K. Zhang, F. Cheng, Z. Tao and J. Chen, *Nanoscale*, 2013, **5**, 6485–6490.
6 Y. Wang, B. Wang, F. Xiao, Z. Huang, Y. Wang, C. Richardson, Z. Chen, L. Jiao and H. Yuan, *J. Power Sources*, 2015, **298**, 203–208.
7 X. Zhou, X. Shen, Z. Xia, Z. Zhang, J. Li, Y. Ma and Y. Qu, *ACS Appl. Mater. Interfaces*, 2015, **7**, 20322–20331.
8 Y. G. Zhu, Y. Wang, Y. Shi, Z. X. Huang, L. Fu and H. Y. Yang, *Adv. Energy Mater.*, 2014, **4**, 1301788.
9 Y. Cao, F. Yuan, M. Yao, J. H. Bang and J.-H. Lee, *CrystEngComm*, 2014, **16**, 826–833.
10 C. Nethravathi, C. R. Rajamathi, M. Rajamathi, X. Wang, U. K. Gautam, D. Golberg and Y. Bando, *ACS Nano*, 2014, **8**, 2755–2765.
11 Y. P. Wang, A. Q. Pan, Q. Y. V. Zhu, Z. W. Nie, Y. F. Zhang, Y. Tang, S. Q. Liang and G. Z. Cao, *J. Power Sources*, 2014, **272**, 107–112.
12 D. Lan, Y. Chen, P. Chen, X. Chen, X. Wu, X. Pu, Y. Zeng and Z. Zhu, *ACS Appl. Mater. Interfaces*, 2014, **6**, 11839–11845.
13 H. Wang, C. Qing, J. Guo, A. A. Aref, D. Sun, B. Wang and Y. Tang, *J. Mater. Chem. A*, 2014, **2**, 11776–11783.
14 S. Liang, J. Zhou, G. Fang, J. Liu, Y. Tang, X. Li and A. Pan, *ACS Appl. Mater. Interfaces*, 2013, **5**, 8704–8709.
15 C. Zheng, C. Cao, Z. Ali and J. Hou, *J. Mater. Chem. A*, 2014, **2**, 16467–16473.
16 W. T. Wei, L. W. Mi, Y. Gao, Z. Zheng, W. H. Chen and X. X. Guan, *Chem. Mater.*, 2014, **26**, 3418–3426.
17 X. F. Gong, J. P. Cheng, K. Y. Ma, F. Liu, L. Zhang and X. B. Zhang, *Mater. Chem. Phys.*, 2016, **173**, 317–324.
18 J. Yang, X. Duan, W. Guo, D. Li, H. Zhang and W. Zheng, *Nano Energy*, 2014, **5**, 74–81.
19 J. Xu, Q. Wang, X. Wang, Q. Xiang, B. Hang, D. Chen and G. Shen, *ACS Nano*, 2013, **7**, 5453–5462.
20 J. Xiao, L. Wan, S. Yang, F. Xiao and S. Wang, *Nano Lett.*, 2014, **14**, 831–838.
21 R. Li, S. L. Wang, Z. C. Huang, F. X. Lu and T. B. He, *J. Power Sources*, 2016, **312**, 156–164.
22 W. Zeng, G. H. Zhang, X. Wu, K. Zhang, H. Zhang, S. C. Hou, C. C. Li, T. H. Wang and H. G. Duan, *J. Mater. Chem. A*, 2015, **3**, 24033–24040.
23 Y. F. Tang, T. Chen, S. X. Yu, Y. Q. Qiao, S. C. Mu, S. H. Zhang, Y. F. Zhao, L. Hou, W. W. Huang and F. M. Gao, *J. Power Sources*, 2015, **295**, 314–322.
24 J. Wang, S. Liu, X. Zhang, X. Liu, X. Liu, N. Li, J. Zhao and Y. Li, *Electrochim. Acta*, 2016, **213**, 663–671.
25 B. Li, Y. X. Hu, J. J. Li, M. C. Liu, L. B. Kong, Y. M. Hu and L. Kang, *Metals*, 2016, **6**, 142.
26 S. H. Choi and Y. C. Kang, *ACS Appl. Mater. Interfaces*, 2015, **7**, 24694–24702.
27 Y. Zheng, T. F. Zhou, C. F. Zhang, J. F. Mao, H. K. Liu and Z. P. Guo, *Angew. Chem., Int. Ed.*, 2016, **55**, 3408–3413.
28 G. Dong, B. Du, L. Liu, W. Zhang, Y. Liang, H. Shi and W. Wang, *Appl. Surf. Sci.*, 2017, **399**, 86–94.
29 X. Chang, T. Wang, P. Zhang, J. Zhang, A. Li and J. Gong, *J. Am. Chem. Soc.*, 2015, **137**, 8356–8359.
30 F. X. Ma, L. Yu, C. Y. Xu and X. W. Lou, *Energy Environ. Sci.*, 2016, **9**, 862–866.
31 X. Y. Yu, L. Yu, L. Shen, X. Song, H. Chen and X. W. Lou, *Adv. Funct. Mater.*, 2014, **24**, 7440–7446.
32 X. Lai, J. E. Halpert and D. Wang, *Energy Environ. Sci.*, 2012, **5**, 5604–5618.
33 X. Sun and Y. Li, *Angew. Chem., Int. Ed.*, 2004, **43**, 597–601.
34 L. Hu, Y. Lu, T. Zhang, T. Huang, Y. Zhu and Y. Qian, *ACS Appl. Mater. Interfaces*, 2017, **9**, 13813–13818.
35 Y. N. Ko and Y. C. Kang, *Carbon*, 2015, **94**, 85–90.
36 J. Wen, S. Li, B. Li, Z. Song, H. Wang, R. Xiong and G. Fang, *J. Power Sources*, 2015, **284**, 279–286.
37 Z. Zhang, Q. Wang, C. Zhao, S. Min and X. Qian, *ACS Appl. Mater. Interfaces*, 2015, **7**, 4861–4868.
38 Y. Zhou, D. Yan, H. Xu, J. Feng, X. Jiang, J. Yue, J. Yang and Y. Qian, *Nano Energy*, 2015, **12**, 528–537.
39 M. Pang, G. Long, S. Jiang, Y. Ji, W. Han, B. Wang, X. Liu, Y. Xi, D. Wang and F. Xu, *Chem. Eng. J.*, 2015, **280**, 377–384.
40 Y. G. Zhu, Y. Wang, Y. Shi, Z. X. Huang, L. Fu and H. Y. Yang, *Adv. Energy Mater.*, 2014, **4**, 1301788.
41 J. Shi, X. Li, G. He, L. Zhang and M. Li, *J. Mater. Chem. A*, 2015, **3**, 20619–20626.
42 H. Hu, B. Y. Guan and X. W. Lou, *Chem*, 2016, **1**, 102–113.
43 H. Li, Y. Gao, Y. Shao, Y. Su and X. Wang, *Nano Lett.*, 2015, **15**, 6689–6695.

44 J. Wen, S. Z. Li, B. R. Li, Z. C. Song, H. N. Wang, R. Xiong and G. J. Fang, *J. Power Sources*, 2015, **284**, 279–286.
45 S. Liu, K. S. Hui, K. N. Hui, J. M. Yun and K. H. Kim, *J. Mater. Chem. A*, 2016, **4**, 8061–8071.
46 L. Yin, L. Wang, X. Liu, Y. Gai, L. Su, B. Qu and L. Gong, *Eur. J. Inorg. Chem.*, 2015, **14**, 2457–2462.
47 J. Deng, L. Kang, G. Bai, Y. Li, P. Li, X. Liu, Y. Yang, F. Gao and W. Liang, *Electrochim. Acta*, 2014, **132**, 127–135.
48 J. Wang, Z. Wang, X. Li, H. Guo, X. Wu, X. Zhang and W. Xiao, *Electrochim. Acta*, 2013, **87**, 224–229.